



Microstructure evolution and mechanical properties of the In–Sn–20Cu composite particles TLP bonding solder joints

Li Yang^{1,3} · Yao Yang^{2,3} · Yaocheng Zhang³ · Feng Xu³ · Jian Qiao^{2,3} · Wangzhang Lu³ · Banglong Yu^{2,3}

Received: 26 December 2019 / Accepted: 4 April 2020 / Published online: 13 April 2020
© Springer-Verlag GmbH Germany, part of Springer Nature 2020

Abstract

In this study, the Cu/In–Sn–20Cu/Cu solder joints were fabricated under the bonding temperature of 260 °C, bonding stress of 3 MPa and bonding time of 0.5–60 min by transient liquid phase bonding. The influence of bonding time on the microstructure evolution and the shear strength of the solder joints was investigated. The results indicated that the intermetallic compound in the interface reaction zone was Cu₃(In, Sn) phase, and its thickness was increased continuously with increasing bonding time. The scallop-type Cu₆(In, Sn)₅ phase was formed at the interface of Cu₃(In, Sn)/In–Sn–20Cu composite solder and then gradually grew to connect the island-type Cu₆(In, Sn)₅ phase which formed in the in situ reaction zone. The transformation of Cu₆(In, Sn)₅ phase to Cu₃(In, Sn) phase occurred in the in situ reaction zone after the bonding time reached 15 min. The shear strength of the Cu/In–Sn–20Cu/Cu solder joints was increased first and then decreased with increasing bonding time. The maximum shear strength was 26.54 MPa when the bonding time reached 15 min. The shear fracture mechanism of solder joints transited from brittle fracture to ductile–brittle mixed fracture with increasing bonding time.

Keywords Transient liquid phase (TLP) bonding · Microstructure evolution · Intermetallic compound (IMC) · Shear strength · Fracture mechanism

1 Introduction

With the development of third-generation semiconductors represented by silicon carbide (SiC) and gallium nitride (GaN), the microelectronic information technology has been widely used in aerospace, automotive, mobile communications, etc. [1–5]. In recent years, the transient liquid phase (TLP) bonding has attracted great attention as a relatively new bonding method applied in the 3D packaging [6, 7]. The method is to form high-melting intermetallic compounds (IMCs) by interdiffusion of metal materials with different

melting temperatures to achieve the connection; the solder joints consisted of the IMCs have superior thermal reliability [8–13].

However, the traditional TLP bonding technology is not suitable for industrial production because most of the solder joints are made in an inert gas and it takes too long to form a dense full IMC solder joint [14, 15]. Hence, new method is developed to improve the traditional TLP bonding techniques. Greve [16] utilized the Cu and Sn powders as a solder paste to shorten the bonding time. The liquid Sn was completely consumed and transformed to Cu₃Sn IMC when the bonding time reached 30 min. But the shear strength of 15 MPa is relatively low due to the existence of a large amount of void. Liu [17] connected Cu–Cu substrate by the mixed nano-Cu particles and flux. The sinterability of micro-Cu particles and the shear strength of solder joints were successfully improved by oxidation–reduction. However, the packaging process is harsh due to the higher bonding stress. Bao [18] employed Sn–Ag mixed particles to fabricate the solder joints and found that the mechanical properties of the solder joints increased first and then decreased with increasing Ag content. The Ag₃Sn IMC solder joints with the maximum shear strength of 72.3 MPa were obtained. However,

✉ Li Yang
linlideyu@126.com

¹ School of Mechanical Engineering, Guilin University of Aerospace Technology, Guilin 541004, People's Republic of China

² School of Mechanical and Electrical Engineering, Soochow University, Suzhou 215000, Jiangsu, People's Republic of China

³ School of Automotive Engineering, Changshu Institute of Technology, Suzhou 215500, Jiangsu, People's Republic of China

the high price of Ag powder led to an increase costs in solder joint fabrication.

Indium metal is widely used in high-tech fields such as electronic computers and aerospace due to its lower melting point (156.6 °C), good fatigue properties, ductility and electrical conductivity [19–23]. Zhao [24] utilized Cu/In/Cu solder joints to bond at 260 °C for 40–360 min and found that the shear strength of the solder joints increased with increasing isothermal solidification time, ranged from 5.08 to 9.07 MPa. The shear strength of the solder joints was low. Sommadossi [25] connected Si/Si at 180 °C by employing Cu and In as the metallization substrate and the intermediate layer solder. It was found that high melting point Cu_2In and Cu_7In_3 phases were formed in the solder joint when the isothermal solidification time was 240 min. However, the shear strength of the solder joints was limited by the Kirkendall voids and cracks at the interface. Kim [26] explored the growth kinetics of the IMC in the Cu/In–48Sn/Cu solder joints during thermal aging. It was found that $\text{Cu}(\text{In}, \text{Sn})_2$ and $\text{Cu}_6(\text{In}, \text{Sn})_5$ IMCs were generated in the interface reaction, and its thickness increased with increasing aging temperature and time.

In this paper, the In–Sn–20Cu composite particle solder was prepared by mixing the micron-sized In, Sn, Cu particles and flux. The Cu/In–Sn–20Cu/Cu solder joints were fabricated under the bonding temperature of 260 °C, bonding stress of 3 MPa and bonding time of 0.5–60 min. The influence of bonding time on microstructure and shear strength of the solder joint was investigated. The shear fracture and the fracture mechanism of the solder joint were analyzed.

2 Experimental procedure

Two pure Cu (99.99 wt%) rods with the dimensions of 10 mm × 10 mm × 4 mm (upper) and 12 mm × 12 mm × 4 mm (bottom) were used as the substrates. In–Sn–20Cu composite particles with the rosin-based flux were employed as interlayer, and the mass fractions of the rosin-based flux were 11.5 wt%. The mass fractions of In particles (3–5 μm), Sn particles (3–5 μm) and Cu particles (10 μm) in In–Sn–20Cu composite particles were 41.6 wt%, 38.4 wt% and 20 wt%, respectively. Micrograph of the In–Sn–20Cu composite particles is shown in Fig. 1. Particles and flux were mixed together under magnetic stirring for 2 h to obtain a homogeneous solder paste. The Cu/In–Sn–20Cu/Cu sandwich TLP bonding solder joints were prepared as shown in Fig. 2.

Cu/In–Sn–20Cu/Cu solder joints were fabricated by a TWB-100 wafer bonder under the bonding temperature of 260 °C, bonding stress of 3 MPa, bonding time of 0.5–60 min and vacuum degree of 1–5 Pa. The microstructure of the solder joints was observed by a German Zeiss Supra 55 scanning electron microscope (SEM)

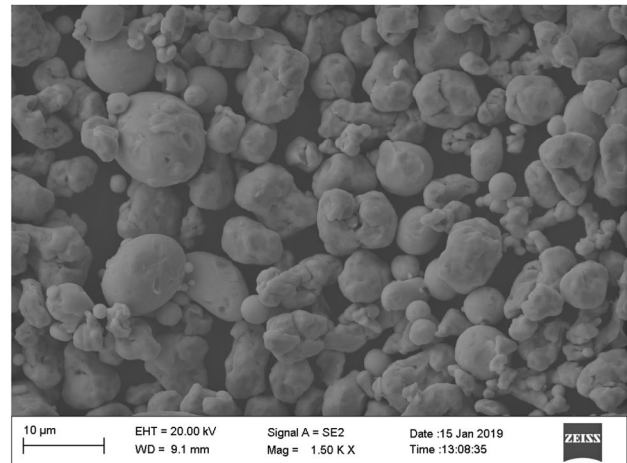


Fig. 1 Micrograph of the In–Sn–20Cu composite particle

equipped with energy-dispersive spectroscopy (EDS). The shear strength of solder joints was tested by the UTM5305 electronic universal testing machine with a shear rate of 0.02 mm/min. The shear strength of the solder joints was estimated by the average value of the three replicate tests; the schematic diagram of shear testing is shown in Fig. 3. X-ray diffraction (XRD) was conducted to identify the main phase on the solder joints, and the shear fracture of the solder joints was observed by SEM.

3 Results and discussion

3.1 Microstructure evolution

Figure 4 shows the microstructure under backscattered electron (BSE) mode of the Cu/In–Sn–20Cu/Cu solder joints bonded under the bonding temperature of 260 °C, bonding stress of 3 MPa and bonding time of 0.5–60 min. Two types of IMCs (layer-type and scallop-type) are observed at the interface of Cu/In–Sn–20Cu solder when the bonding time is 0.5 min (Fig. 4a). Based on the EDS results (Table 1), the layer-type IMC on the Cu side is $\text{Cu}_3(\text{In}, \text{Sn})$, and the scallop-type IMC on the solder side is $\text{Cu}_6(\text{In}, \text{Sn})_5$. The diffusion reaction is further strengthened with increasing bonding time, which leads to the increment of the $\text{Cu}_3(\text{In}, \text{Sn})$ IMC layer thickness. The block-type $\text{Cu}_6(\text{In}, \text{Sn})_5$ IMC phase is formed by the growth of the scallop-type $\text{Cu}_6(\text{In}, \text{Sn})_5$ IMC phases and the connection between the scallop-type $\text{Cu}_6(\text{In}, \text{Sn})_5$ IMC phases and the island-type $\text{Cu}_6(\text{In}, \text{Sn})_5$ IMC phases when the bonding time reaches 5 min (Fig. 4b, c).

It can see that a small amount of Cu particles are entrapped by $\text{Cu}_3(\text{In}, \text{Sn})$ phase in the in situ reaction zone when the bonding time reaches 15 min (Fig. 4d). Because

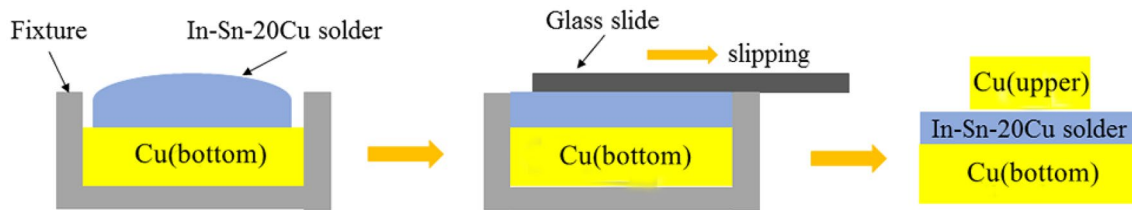


Fig. 2 Schematic illustration of the Cu/In–Sn–20Cu/Cu solder joints preparation

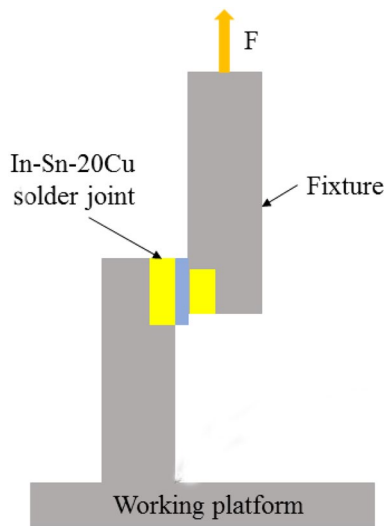
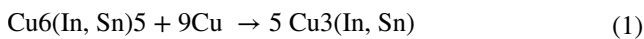


Fig. 3 Schematic diagram of shear testing of the solder joints

the gap of the Cu particles in the solder is filled with the melted In and Sn particles at the bonding temperature of 260 °C. The Cu particles and the surrounded liquid In, Sn gradually form the Cu₆(In, Sn)₅ phase, and then, the transformation of Cu₆(In, Sn)₅ phase to Cu₃(In, Sn) phase occurs in the in situ reaction zone. There is one reaction for this transformation, as shown in reaction (1):



In order to determine the volume change caused by the phase transformation, a theoretical calculation is performed. The volume change before and after the reaction (1) is shown in Eq. (2):

$$\begin{aligned} \Delta V &\equiv V_{\text{Cu}_6(\text{In, Sn})_5} + 9V_{\text{Cu}} - 5V_{\text{Cu}_3(\text{In, Sn})} \\ &= \frac{6M_{\text{Cu}} + 5M_{\text{Sn}} + 5M_{\text{In}}}{\rho_{\text{Cu}_6(\text{In, Sn})_5}} + \frac{9M_{\text{Cu}}}{\rho_{\text{Cu}}} - \frac{5(3M_{\text{Cu}} + M_{\text{In}} + M_{\text{Sn}})}{\rho_{\text{Cu}_3(\text{In, Sn})}} \end{aligned} \quad (2)$$

where ΔV is volume change, M_{Cu} , M_{Sn} and M_{In} are the molar mass of Cu, Sn and In, $\rho_{\text{Cu}_3(\text{In, Sn})}$, $\rho_{\text{Cu}_6(\text{In, Sn})_5}$ and ρ_{Cu} are the density of Cu₃(In, Sn), Cu₆(In, Sn)₅ and Cu. Based on Eq. (2), the ΔV is calculated as 3.18 cm³. According to the calculation results, it is found that the volume shrinks

after the transformation of Cu₆(In, Sn)₅ phase to Cu₃(In, Sn) phase. The volume shrinkage forms a large amount of contraction voids (Fig. 4d).

It can see that the island-type Cu₆(In, Sn)₅ phase gradually decreased, the layer-type Cu₃(In, Sn) phase increased and the Cu particles disappeared after the bonding time reached 30 min (Fig. 4e–f). Therefore, a full IMC solder joint composed of a large amount of Cu₃(In, Sn) and a small amount of Cu₆(In, Sn)₅ is formed. Meanwhile, some Kirkendall voids are found at the interface of Cu/Cu₃(In, Sn) in the solder joint, as shown in Fig. 4e–f. The Cu atoms in the in situ reaction zone are completely consumed by reaction (1), and the Cu atoms on the substrate diffuse through the gap of Cu₃(In, Sn) IMCs by the capillary action. When the solder joint is affected by temperature, the thermal expansion coefficients will be different due to the different IMC phases, and the mismatch of thermal expansion coefficients will cause constraints between the phases, which will restrict each other. The surrounding area is sharply heated by the capillary action of the diffusion of Cu atoms. During the cooling process after the bonding is completed, the cooling shrinkage of the phase will be constrained by the residual thermal stress. Eventually, it leads to the formation of voids in the Cu₃(In, Sn) IMC layer [27].

The diffusion process of Cu atoms in the solid Cu substrate is carried out under the action of diffusion driving force, and the diffusion process is carried out along the direction in which the Cu concentration is lowered, so that the concentration tends to be uniform. From the thermodynamic view, the free energy of the solder joint can be reduced by the spontaneous migration of the constituent atoms from a high chemical position to a low chemical position under isothermal and isostatic conditions.

When the bonding time is short (0.5–5 min), the concentration of Cu in the Cu/In–Sn–20Cu interface is not balanced, and a large amount of diffusion reaction occurs to form the Cu₃(In, Sn) phase. The concentration of Cu atoms on both sides of the interface is temporarily balanced with the in situ reaction and more diffusion reaction. The consumption of Cu atoms is promoted according to the reaction (1) after the bonding time reaches 15 min. The unbalanced diffusion of Cu atoms from the substrate passes through the

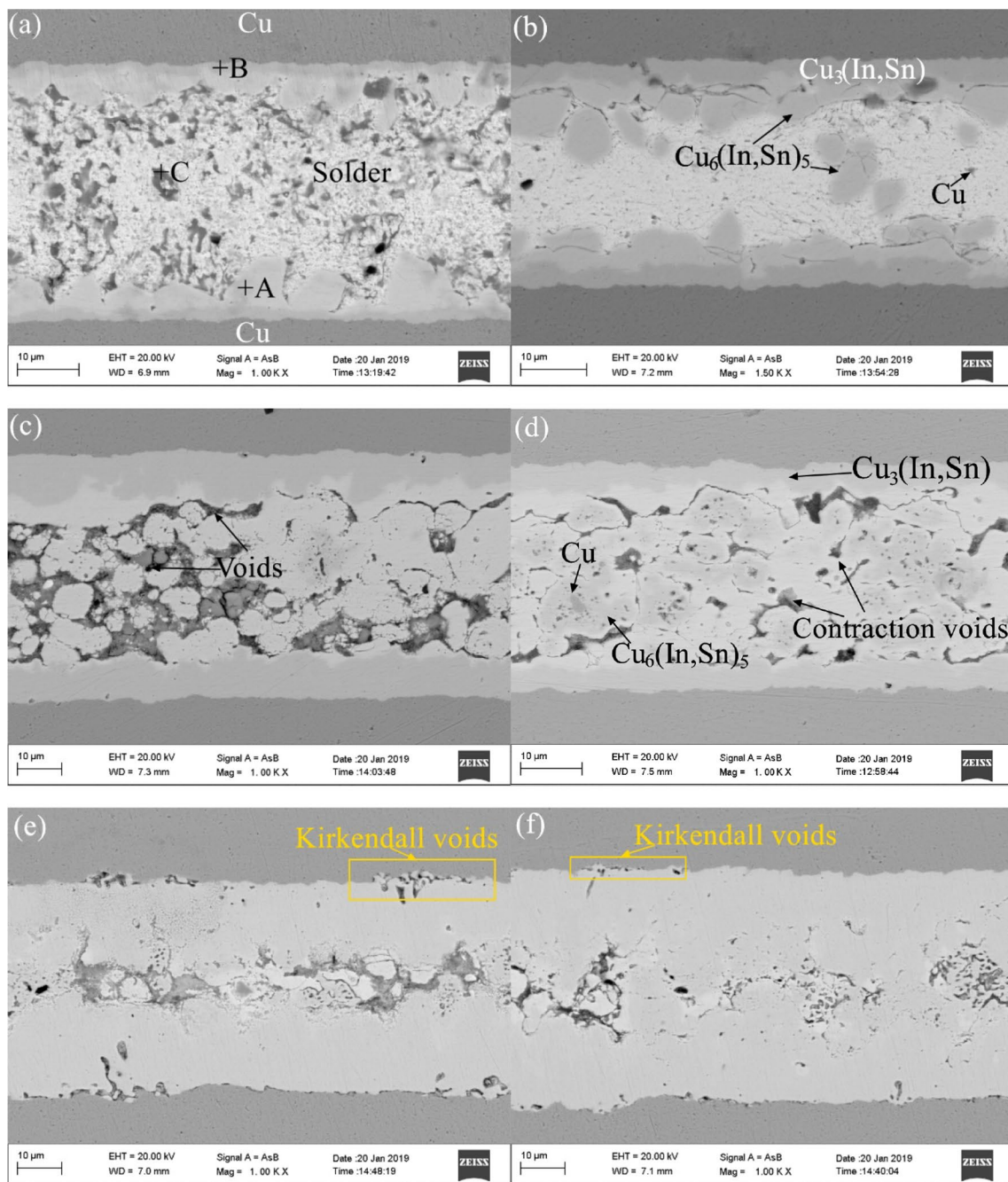


Fig. 4 The microstructure under backscattered electron (BSE) mode of the Cu/In–Sn–20Cu/Cu solder joints bonded under the bonding temperature of 260 °C, bonding stress of 3 MPa and bonding time of **a** 0.5 min, **b** 1 min, **c** 5 min, **d** 15 min, **e** 30 min, **f** 60 min

Table 1 EDS analysis results of the indicated areas in Fig. 3a

Elemental composition (at.%)				
Area	In	Sn	Cu	Phase
A	23.52	22.01	54.47	Cu ₆ (In, Sn) ₅
B	12.51	11.75	75.74	Cu ₃ (In, Sn)
C	1.56	0.73	97.71	Cu

Cu₃(In, Sn) phase framework gap by capillary action, which produces Kirkendall voids [28].

3.2 Shear strength

Figure 5 shows the shear strength of the Cu/In–Sn–20Cu/Cu solder joints bonded under the bonding temperature of 260 °C, bonding stress of 3 MPa and bonding time of

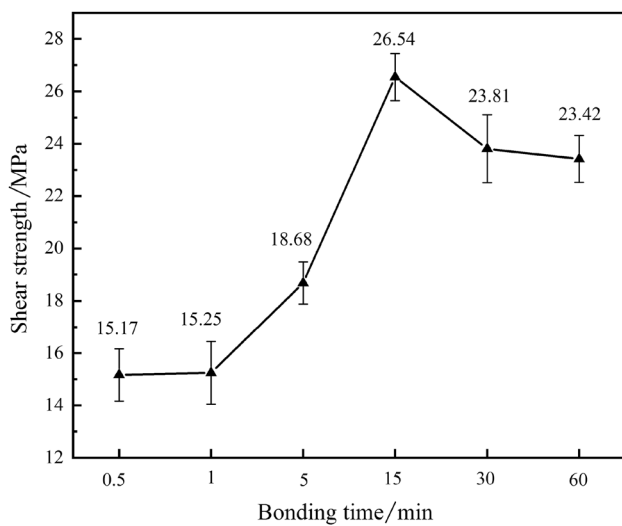


Fig. 5 The shear strength of the Cu/In–Sn–20Cu/Cu solder joints bonded under the bonding temperature of 260 °C, bonding stress of 3 MPa and bonding time of 0.5–60 min

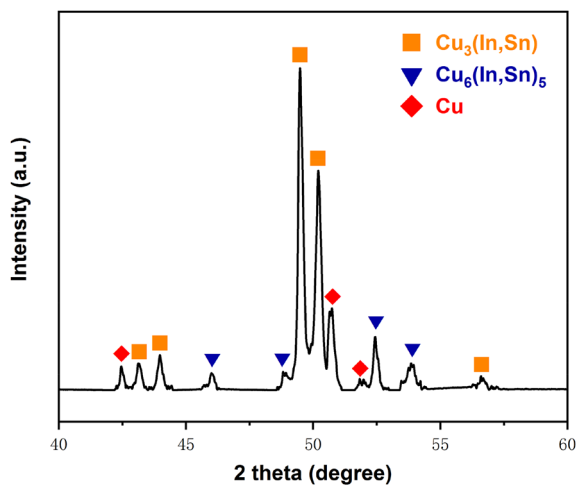


Fig. 6 The XRD analysis of the Cu/In–Sn–20Cu/Cu solder joint bonded for 15 min

0.5–60 min. The shear strength is increased first and then decreased with increasing bonding time, and the maximum shear strength is 26.54 MPa when the bonding time is 15 min. According to the microstructure evolution, the solder joint mainly consists of $\text{Cu}_3(\text{In, Sn})$ and $\text{Cu}_6(\text{In, Sn})_5$ IMCs. The thickness of $\text{Cu}_3(\text{In, Sn})$ IMC layer is gradually increased, and the $\text{Cu}_6(\text{In, Sn})_5$ IMC expands into a large block with increasing bonding time, which indicates that the both IMCs can improve the shear strength of the solder joint. The Cu atoms diffused from the Cu substrate are dispersed in the solder joint bonded for 15 min, which makes the solder joint densified. The XRD results shown in Fig. 6 prove that the joint is composed of the $\text{Cu}_3(\text{In, Sn})$,

$\text{Cu}_6(\text{In, Sn})$ and Cu when the bonding time is 15 min. Bosco [29] has demonstrated that the dispersion of Cu atoms in the intergranular compound distributed grain boundaries can enhance the strength and ductility of TLP solder joints. The presence of a large amount of Cu atoms can alleviate the stress concentration, absorb partial tensile stress during shearing to enhance the mechanical properties of the solder joint.

The Cu/In–Sn–20Cu/Cu solder joint bonded for 30–60 min exhibits full IMCs of $\text{Cu}_3(\text{In, Sn}) + \text{Cu}_6(\text{In, Sn})_5$. The solder joint breaks easily during the shear process due to the brittleness exhibited by the full IMCs, which results in a continuous decrease in shear strength. In addition, the unreacted liquid In and Sn are separated into some isolated areas by the porous skeleton of the $\text{Cu}_3(\text{In, Sn})$ IMC phase formed in the in situ reaction zone, and a large amount of voids are formed by volume shrinkage of the solidification during the bonding process.

3.3 Shear fracture

Figure 7 shows the fracture morphologies of the Cu/In–Sn–20Cu/Cu solder joints bonded under the bonding temperature of 260 °C, bonding stress of 3 MPa and bonding time of 0.5–60 min. Many dimples and $\text{Cu}_6(\text{In, Sn})_5$ IMC are observed at the fracture surface of the Cu/In–Sn–20Cu/Cu solder joint bonded for 0.5 min (Fig. 7a), which indicates that the fracture occurs between In–Sn–20Cu solder and $\text{Cu}_6(\text{In, Sn})_5$ IMC. A large number of the needle-type $\text{Cu}_3(\text{In, Sn})$ phases are observed at the fracture surface (Fig. 7b) when bonding time reaches 5 min. The tear and plastic deformation of the $\text{Cu}_3(\text{In, Sn})$ IMCs indicates that the fracture occurs on $\text{Cu}_3(\text{In, Sn})$ layers of the solder joint. The same characteristics of the step type are found at the two fractures, indicating that the fracture mechanism is brittle fracture.

Many honeycomblike structure is observed at the fractures of the solder joint bonded for 15 and 60 min (Fig. 7c, d). The fracture structure is mainly composed of the $\text{Cu}_3(\text{In, Sn})$ phase and a large amount of spherical-type $\text{Cu}_6(\text{In, Sn})_5$ phase, indicating that the fracture occurs in the interfacial reaction zone. The shear fracture mechanism of solder joints transits from brittle fracture to ductile–brittle mixed fracture when the bonding time reaches 60 min. Due to the poor strength of $\text{Cu}_6(\text{In, Sn})_5$ and the contraction voids generated by the phase transformation of $\text{Cu}_6(\text{In, Sn})_5$ phase to $\text{Cu}_3(\text{In, Sn})$ phase, the cracks initiate at the voids and propagate through the $\text{Cu}_6(\text{In, Sn})_5$ phase quickly under the stress concentration during the shearing process (Fig. 8). As a consequence, the fracture path forms in the in situ reaction zone and the fracture morphology displays a few spherical-type $\text{Cu}_6(\text{In, Sn})_5$ phases adhered to $\text{Cu}_3(\text{In, Sn})$ phase.

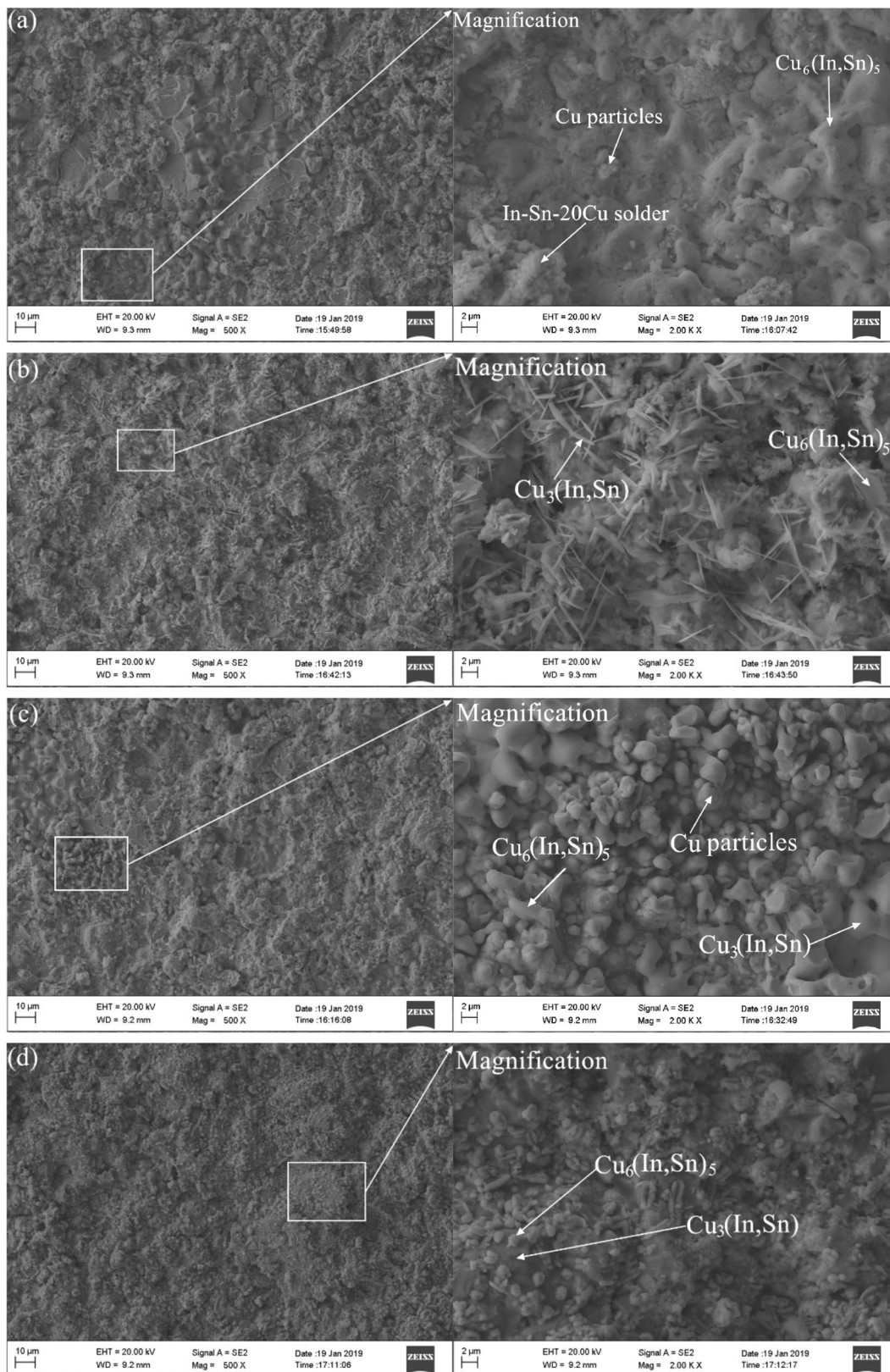


Fig. 7 The fracture surfaces of the Cu/In-Sn-20Cu/Cu solder joints bonded under the bonding temperature of 260 °C, bonding stress of 3 MPa and bonding time of **a** 0.5 min, **b** 5 min, **c** 15 min, **d** 60 min

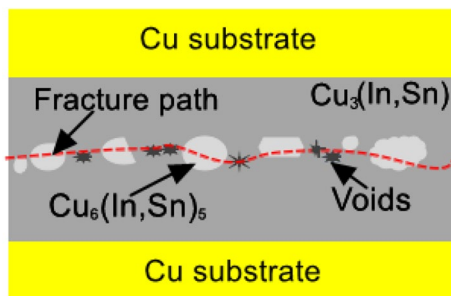


Fig. 8 Illustration of fracture path in the Cu/In–Sn–20Cu/Cu solder joints bonded for 60 min

4 Conclusions

In this work, the influence of bonding time on microstructure evolution and shear strength of the Cu/In–Sn–20Cu/Cu solder joint under the bonding temperature of 260 °C, bonding stress of 3 MPa and bonding time of 0.5–60 min was investigated. The fracture morphologies and the reason of voids formation were also discussed. According to the experimental analyses, the conclusions are summarized as follows:

- (1) The IMCs of the Cu/In–Sn–20Cu/Cu solder joint consist of $\text{Cu}_3(\text{In, Sn})$ and $\text{Cu}_6(\text{In, Sn})_5$ during the bonding process. The conversion of the $\text{Cu}_6(\text{In, Sn})_5$ phase to the $\text{Cu}_3(\text{In, Sn})$ phase has occurred gradually with increasing bonding time. A full IMC solder joint is eventually formed by the increment of the $\text{Cu}_3(\text{In, Sn})$ IMC layer thickness, the reduction of the island-type $\text{Cu}_6(\text{In, Sn})_5$ phase and consumption of Cu atoms.
- (2) The volume shrinkage by the transformation of $\text{Cu}_6(\text{In, Sn})_5$ phase to $\text{Cu}_3(\text{In, Sn})$ phase causes a large amount of contraction voids in the in situ reaction zone with increasing bonding time. The generation of Kirkendall voids at the interface of $\text{Cu}_3(\text{In, Sn})/\text{Cu}$ is the unbalanced diffusion result of the Cu atoms from the substrate after the bonding time reaches 30 min.
- (3) The shear strength of the solder joints increases first and then decreases with increasing bonding time. The maximum shear strength is 26.54 MPa when the bonding time is 15 min. The shear fracture mechanism of the solder joints transits from brittle fracture to ductile–brittle mixed fracture after the bonding time reaches 60 min.

Acknowledgements This research was financially supported by the National Natural Science Foundation of China (51865006) and Natural Science Foundation of the Jiangsu Higher Education Institutions of China (19KJA430001, 18KJA460001).

References

1. S. Sakamoto, T. Sugahara, K. Suganuma, Microstructural stability of Ag sinter joining in thermal cycling. *J. Mater. Sci. Mater. Electron.* **24**, 1332–1340 (2012)
2. L.A. Navarro, X. Perpina, P. Godignon, J. Montserrat, V. Banu, M. Vellvehi, X. Jorda, Thermomechanical assessment of die-attach materials for wide bandgap semiconductor devices and harsh environment applications. *IEEE Trans. Power Electron.* **29**, 2261–2271 (2014)
3. Q. Guo, S.Y. Sun, Z.H. Zhang, H.T. Chen, M.Y. Li, Microstructure evolution and mechanical strength evaluation in Ag/Sn/Cu TLP bonding interconnection during aging test. *Microelectron. Reliab.* **80**, 144–148 (2018)
4. L. Zhang, Z.Q. Liu, S.W. Chen, Y.D. Wang, W.M. Long, Y.H. Guo, S.Q. Wang, Y. Guo, W.Y. Liu, Materials, processing and reliability of low temperature bonding in 3D chip stacking. *J. Alloys Compd.* **750**, 980–995 (2018)
5. H.K. Shao, A.P. Wu, Y.D. Bao, Y. Zhao, L. Liu, G.S. Zou, Rapid Ag/Sn/Ag transient liquid phase bonding for high-temperature power devices packaging by the assistance of ultrasound. *Ultrason. Sonochem.* **37**, 561–570 (2017)
6. W.Y. Chen, R.W. Song, J.G. Duh, Grain structure modification of Cu–Sn IMCs by applying Cu–Zn UBM on transient liquid-phase bonding in novel 3D-IC technologies. *Intermetallics* **85**, 170–175 (2017)
7. K. Bobzin, N. Bagcivan, L.D. Zhao, S. Ferrara, J. Perne, Development of new transient liquid phase system Au–Sn–Au for microsystem technology. *Front. Mech. Eng. China* **5**, 370–375 (2010)
8. L. Sun, M.H. Chen, L. Zhang, Microstructure evolution and grain orientation of IMC in Cu–Sn TLP bonding solder joints. *J. Alloys Compd.* **786**, 677–687 (2019)
9. H.K. Shao, A.P. Wu, Y.D. Bao, Y. Zhao, G.S. Zou, L. Liu, Microstructure evolution and mechanical properties of Cu/Sn/Ag TLP-bonded joint during thermal aging. *Mater. Charact.* **144**, 469–478 (2018)
10. O. Mokhtari, H. Nishikawa, The shear strength of transient liquid phase bonded Sn–Bi solder joint with added Cu particles. *Adv. Powder Technol.* **27**, 1000–1005 (2016)
11. M. Brincker, S. Söhl, R. Eisele, V.N. Popok, Strength and reliability of low temperature transient liquid phase bonded Cu–Sn–Cu interconnects. *Microelectron. Reliab.* **76–77**, 378–382 (2017)
12. H.K. Shao, A.P. Wu, Y.D. Bao, Y. Zhao, L. Liu, G.S. Zou, Interactions at the planar $\text{Ag}_3\text{Sn}/\text{liquid Sn}$ interface under ultrasonic irradiation. *Ultrason. Sonochem.* **39**, 758–764 (2017)
13. H.K. Shao, A.P. Wu, Y.D. Bao, Y. Zhao, G.S. Zou, L. Liu, Thermal reliability investigation of Ag–Sn TLP bonds for high-temperature power electronics application. *Microelectron. Reliab.* **91**, 38–45 (2018)
14. Z.J. Wu, J. Cai, Q. Wang, Q. Wang, J.Q. Wang, D.J. Wang, Wafer-level hermetic package by low-temperature Cu/Sn TLP bonding with optimized Sn thickness. *J. Electron. Mater.* **46**, 6111–6118 (2017)
15. F.Q. Lang, H. Yamaguchi, H. Nakagawa, H. Sato, in *IEEE 13th International Conference on Electronic Packaging Technology and High Density Packaging (ICEPT-HDP)*, (2012), pp. 157–161
16. H. Greve, S.A. Moeini, P. McCluskey, S. Joshi, Prediction and mitigation of vertical cracking in high-temperature transient liquid phase sintered joints by thermomechanical simulation. *J. Electron. Packag.* **140**, 020903 (2018)
17. X.D. Liu, H. Nishikawa, Low-pressure Cu–Cu bonding using in situ surface-modified microscale Cu particles for power device packaging. *Scr. Mater.* **120**, 80–84 (2016)

18. Y.D. Bao, A.P. Wu, H.K. Shao, Y. Zhao, L. Liu, G.S. Zou, Microstructural evolution and mechanical reliability of transient liquid phase sintered joint during thermal aging. *J. Mater. Sci.* **54**, 765–776 (2018)
19. L.L. Yan, C.K. Lee, D.Q. Yu, W.K. Choi, A. Yu, S.U. Yoon, J.H. Lau, in *58th Electronic Components and Technology Conference (ECTC)*, (2008), pp. 1844–1848
20. C.A. Yang, S. Yang, X. Liu, H. Nishikawa, C.R. Kao, Enhancement of nano-silver chip attachment by using transient liquid phase reaction with indium. *J. Alloys Compd.* **762**, 586–597 (2018)
21. W.K. Choi, C.S. Premachandran, O.S. Chiew, X. Lin, L. Ebin, A. Khairyanto, B. Ratmin, C.W.S. Kelvin, P. P. Thaw, J.H. Lau, in *59th Electronic Components and Technology Conference (ECTC)*, (2009), pp. 333–338
22. Y. Li, A.B.Y. Lim, K.M. Luo, Z. Chen, F.S. Wu, Y.C. Chan, Phase segregation, interfacial intermetallic growth and electromigration-induced failure in Cu/In–48Sn/Cu solder interconnects under current stressing. *J. Alloys Compd.* **673**, 372–382 (2016)
23. X.C. Xie, C.J. Hang, J.Q. Wang, Y. Su, J. Ma, Q. Guo, H.T. Chen, M.Y. Li, A low temperature die attach technique for high temperature applications based on indium infiltrating micro-porous Ag sheet. *J. Mater. Sci. Mater. Electron.* **29**(21), 18302–18310 (2018)
24. X. Zhao, Y.H. Tian, N. Wang, in *IEEE 14th International Conference on Electronic Packaging Technology and High Density Packaging (ICEPT-HDP)*, (2013), pp. 143–147
25. S. Sommadossi, L. Litynska, P. Zieba, W. Gust, E.J. Mittemeijer, Transmission electron microscopy investigation of the microstructure and chemistry of Si/Cu/In/Cu/Si interconnections. *Mater. Chem. Phys.* **81**, 566–568 (2003)
26. D.G. Kim, S.B. Jung, Interfacial reactions and growth kinetics for intermetallic compound layer between In–48Sn solder and bare Cu substrate. *J. Alloys Compd.* **386**, 151–156 (2005)
27. H.K. Shao, A.P. Wu, Y.D. Bao, Y. Zhao, G.S. Zou, L. Liu, Novel transient liquid phase bonding through capillary action for high-temperature power devices packaging. *Mater. Sci. Eng. A* **724**, 231–238 (2018)
28. Y.D. Bao, A.P. Wu, H.K. Shao, Y. Zhao, G.S. Zou, Effect of powders on microstructures and mechanical properties for Sn–Ag transient liquid phase bonding in air. *J. Mater. Sci. Mater. Electron.* **29**(12), 10246–10257 (2018)
29. N.S. Bosco, F.W. Zok, Strength of joints produced by transient liquid phase bonding in the Cu–Sn system. *Acta Mater.* **53**(7), 2019–2027 (2005)

Publisher's Note Springer Nature remains neutral with regard to jurisdictional claims in published maps and institutional affiliations.